Polymer 49 (2008) 3795–3804

Contents lists available at ScienceDirect

Polymer

journal homepage: www.elsevier.com/locate/polymer

Effect of organoclay structure on morphology and properties of nanocomposites based on an amorphous polyamide

Youngjae Yoo, D.R. Paul*

Department of Chemical Engineering, Texas Materials Institute, The University of Texas at Austin, Austin, TX 78712, United States

ARTICLE INFO

Article history:
Received 6 March 2008
Received in revised form 10 June 2008
Accepted 11 June 2008
Available online 14 June 2008

Keywords:
Amorphous polyamide
Nanocomposites
Organoclays

ABSTRACT

An amorphous polyamide (a-PA) and three organoclays, $M_3(HT)_1$, $M_2(HT)_2$ and $(HE)_2M_1T_1$, were melt processed to explore the effect of the organoclay structure on the extent of exfoliation and properties of these nanocomposites. Wide angle X-ray scattering, transmission electron microscopy, and stress–strain behavior were used to determine the degree of exfoliation of the nanocomposites. For quantitative assessment of the structure of the nanocomposites, a detailed particle analysis was made to provide various averages of the clay dimensions and aspect ratio. The results evaluated from different methods were generally consistent with each other. Nanocomposites based on the organoclays with one alkyl tail and hydroxyl ethyl groups gave well-exfoliated structures and high matrix reinforcement while nanocomposites from two-tailed organoclay contain a considerable concentration of intercalated stacks. Nanocomposites from the organoclays with one alkyl tail showed slightly better exfoliation and matrix reinforcement than those from the organoclays with hydroxyl ethyl groups. The organoclay structure trends for a-PA are analogous to what has been observed for nylon 6; this suggests that a-PA, like nylon 6, has good affinity for the pristine silicate surface of the clay leading to better exfoliation and enhanced mechanical properties with one-tailed organoclay than multiple-tailed organoclay. Furthermore, heat distortion temperatures were predicted from the dynamic mechanical properties of nanocomposites.

1. Introduction

Polymer nanocomposites based on organoclays as a filler offer improved performance and opportunities for commercial applications [1,2]. The key to significant enhancement in properties is to exfoliate the individual organoclay platelets into the polymer matrix to utilize their high aspect ratio and modulus [3,4]. The affinity between polymer matrix and organoclay is one of the most important factors in achieving good exfoliation; to a certain extent the affinity can be enhanced by optimizing the structure of the organoclay for a given polymer matrix. Previous studies have shown that semi-crystalline polyamides like nylon 6, nylon 66, nylon 11, nylon 12, etc. give rather good exfoliation [5–10]. The best exfoliation is obtained with organoclays based on one long alkyl tail apparently owing to the affinity of polyamides for the silicate surface; organoclays based on one long alkyl tail provide more access to the silicate surface of the clay than two or more alkyl tails [8,9,11]. The opposite is true for nonpolar polymers such as polyolefins where the interaction with the silicate surface is poor, and, thus, more alkyl tails is preferable since this blocks the unfavorable silicate/polyolefin interaction and increases the alkyl/polyolefin contacts [12–15].

Here we examine the formation and the properties of nanocomposites based on an amorphous polyamide, Zytel® 330 from DuPont, designated as a-PA. This engineering polymer has favorable properties including good dimensional stability, good dielectric properties, and resistance to oxygen and other chemicals [16–18]. However, there are very few reports on nanocomposites based on a-PA prepared by melt mixing [19,20] in spite of the obvious advantages of this approach [3,4,21–26].

The aim of this paper is to investigate the morphology and properties of nanocomposites based on a-PA and their relationship to the structure of the organic modifier used to form the organoclays. This paper also provides background data for a subsequent paper about rubber toughening of a-PA nanocomposites. Since a-PA is a pseudo-ductile material with a low notched Izod impact strength, significant toughening can be achieved by forming rubber particles of controlled sizes [27,28]. Rubber toughening of nanocomposites is a potential route to a unique balance between toughness, strength and other properties [14,29–32].

* Corresponding author. Tel.: +1 512 471 5392; fax: +1 512 471 0542.
E-mail address: drp@che.utexas.edu (D.R. Paul).

0032-3861/$ – see front matter © 2008 Elsevier Ltd. All rights reserved.
doi:10.1016/j.polymer.2008.06.014

Table 1
Materials used in this study

Material (designation in this paper)	Commercial designation	Specifications	Supplier
Polymer			
a-PA[a]	Zytel® 330	[COOH]/[NH2] = 4.5,[b] T_g = 127 °C $\overline{M}_n$ = 14,000,[c] $\overline{M}_w$ = 50,000[c]	DuPont
Organoclays[d]			
$M_3(HT)_1$	*Experimental*: Trimethyl hydrogenated tallow ammonium montmorillonite	Organic loading = 95 mequiv/100 g clay Organic content = 29.6 wt% d_{001} spacing = 18.0 Å[e]	Southern Clay Products
$M_2(HT)_2$	*Cloisite® 20A*: Dimethyl bis(hydrogenated tallow) ammonium montmorillonite	Organic loading = 95 mequiv/100 g clay Organic content = 39.6 wt% d_{001} spacing = 24.2 Å[e]	Southern Clay Products
$(HE)_2M_1T_1$	*Cloisite® 30B*: Bis(2-hydroxy-ethyl)methyl tallow ammonium montmorillonite	Organic loading = 90 mequiv/100 g clay Organic content = 31.5 wt% d_{001} spacing = 17.9 Å[e]	Southern Clay Products

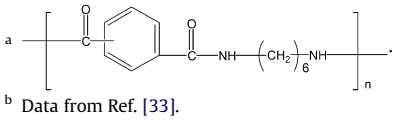

[b] Data from Ref. [33].
[c] Data from Ref. [45].
[d] The selected organoclay is designated as $M_2(HT)_2$ in this study, where M = methyl, HT = hydrogenated tallow and HE = hydroxy-ethyl. Tallow is a natural product composed predominantly (63%) of saturated and unsaturated C_{18} chains. HT is the saturated form yet still contains a small fraction of double bonds.
[e] The basal spacing corresponds to the characteristic Bragg reflection peak d_{001} obtained from a powder WAXS scan of the organoclay.

2. Experimental

2.1. Materials

Table 1 summarizes the materials used in this study. The amorphous polyamide, a-PA, chosen for this study, Zytel® 330, was supplied by DuPont. It has a glass transition temperature of 127 °C and a number average molecular weight of 14,000. The chains of a-PA are rich in [COOH] groups [33], i.e., $[COOH]/[NH_2] = 4.5$ as shown in Table 1. This result is somewhat unusual, since typical polyamides such as nylon 6 or nylon 66 have balanced [COOH] and $[NH_2]$ groups, i.e., $[COOH]/[NH_2] \approx 1$, unless the polyamide is made to be rich in one or the other end-groups for some particular purpose [28]. Three kinds of organoclays from Southern Clay Products were formed by cation exchange reaction between Na^+MMT and various organic modifiers as described elsewhere [3,8,11,34]. The nomenclature system, defined in previous reports [3,8,11,12,15,21,34,35], uses various abbreviations to represent the substituents on the cation, e.g., M for methyl, H for hydrogen and HE for 2-hydroxyl-ethyl while T and HT represent long alkyl chains from natural tallow oil and hydrogenated tallow, respectively. The organoclays were selected to investigate the effects of the organic modifier structure on the dispersion of organoclay platelets in the a-PA matrix. Comparison of $M_3(HT)_1$ and $(HE)_2M_1T_1$ explores the effect of a number of alkyl tails while comparison of $M_3(HT)_1$ and $M_2(HT)_2$ examines the effect of hydroxyl groups.

2.2. Melt processing

Prior to melt processing, Zytel® 330 was dried for a minimum of 48 h in a vacuum oven at 65 °C while the organoclay was used as-received. Blending was accomplished in a Haake co-rotating, intermeshing twin-screw extruder (diameter = 30 mm, $L/D = 10$) using a barrel temperature of 240 °C, a screw speed of 280 rpm. The a-PA and organoclay mixture were divided into four 300 g batches each and dry blended for minimizing non-uniformity of feeding. Dry blended materials were introduced into a solid screw feeder and fed into the extruder at a rate of 1200 g/h in a "starve feed" mode to make total batch of 1 kg. The pellets from the extrusion compounding mixed there were dried again in a vacuum oven and molded into standard tensile (ASTM D638, Type I) and Izod (ASTM D256) bars (0.318 cm thick) via an Arburg All-rounder 305-210-700 injection molding machine using a barrel temperature of 240 °C, mold temperature of 80 °C, injection pressure of 70 bar and a holding pressure of 35 bar. The resulting specimens were tested 'dry as-molded'.

2.3. Characterization

Morphology was examined via a JEOL 2010F transmission electron microscope (TEM) operating under an accelerating voltage of 120 kV. Samples for morphology analysis were taken from the core portion of an injection-molded bar. Ultra-thin sections of approximately 50 nm thickness were cryogenically cut with a diamond knife while cooled using liquid nitrogen at a temperature of −40 °C using an RMC PowerTome XL microtome. These sections were taken from the plane defined by the flow direction (FD) and the normal direction (ND) of the molded bar as explained elsewhere [36]. Sections were collected using 300 mesh grids and dried using filter paper.

Wide angle X-ray scattering (WAXS) was performed using a Scintag XDS 2000 diffractometer in the reflection mode, using an incident X-ray wavelength of 0.154 nm at a scan rate of 1.0°/min. The three corresponding organoclays used in this work, i.e., $M_3(HT)_1$, $M_2(HT)_2$ and $(HE)_2M_1T_1$, were scanned in the form of powder while injection-molded samples of nanocomposites formed from them were also scanned such that the beam probed the skin of an Izod bar perpendicular to the FD. For certain samples, identified as such in the text, the skin of the bar was removed by an automated milling machine prior to the WAXS scans in order to obtain information about the morphology in the core of the bar.

Tensile tests were performed according to ASTM D638 using an Instron model 1137 testing machine upgraded for computerized data acquisition. Values of the tensile modulus were determined using an extensometer. Modulus and yield strength data were determined at a crosshead rate of 0.51 cm/min. Elongation at break results were taken at 5.1 cm/min. Izod impact tests were conducted using a 6.8 J hammer and 3.5 m/s impact velocity at room temperature using a TMI Impact tester (model 43-02). Standard notches were made according to ASTM D256. Typically, data from at least five specimens were averaged to determine mechanical properties.

The dynamic mechanical properties of nanocomposites were determined by a Rheometric Scientific Dynamic Mechanical Thermal Analyzer (DMTA) Mk III at a frequency of 1 Hz, a strain level setting of 4 which corresponds to about 0.07% strain, and under a single cantilever mode. Injection-molded (0.318 cm thick) specimens of neat a-PA and nanocomposites employed in this work were heated from 30 to 135 °C at a rate of 2 °C/min and analyzed for storage modulus (E') and tan δ. The heat distortion temperature, HDT, for these materials was estimated from the relationship between $\log E'$ and temperature using a technique proposed by Scobbo [37].

2.4. Particle analysis

Particle analysis was performed on TEM micrographs, typically at 15K magnification, for each sample. For accurate particle analysis, TEM micrographs were saved and converted into .jpg format. Quantitative particle analysis was performed by opening a saved digital file in Adobe Photoshop where the dispersed platelets and/or agglomerates are traced over an overlapped blank layer. To ensure accurate measurements of the particle length and thickness, the image is sufficiently magnified so that most of the particles, including single platelets, are counted. The resulting black/white layer file is imported into the image analysis program, SigmaScan Pro, used to analyze the traced particles in terms of both length and thickness. Using the software, each particle was assigned a numerical label and exported to separate files [13,21]. To ensure statistical validity of the analysis, 200–900 particles were counted to measure the length, thickness, and actual aspect ratio of particles for nanocomposites. The results are summarized in Table 2. In this study, four different kinds of aspect ratios are introduced, i.e., the number and weight averages of the aspect ratios calculated for individual ***particles, $\langle l/t\rangle_n$ and $\langle l/t\rangle_w$, and ratios of the number and weight averages of particle lengths and thicknesses, $(\bar{l}_n/\bar{t}_n)$ and $(\bar{l}_w/\bar{t}_w)$.

3. Results and discussion

3.1. Morphology

3.1.1. Transmission electron microscopy

TEM observations for nanocomposites were performed to qualitatively assess the degree of organoclay exfoliation in the polymer matrix. Fig. 1 shows representative TEM micrographs for nanocomposites with different MMT concentrations. All micrographs were taken from the plane defined by the flow direction (FD) and the normal direction (ND) of the molded bar. At low MMT concentrations, micrographs of all the nanocomposites reveal well-exfoliated structures containing dispersed layer(s) of MMT, in which individual MMT platelets are easily observed. However, at higher MMT concentrations, nanocomposites from $M_2(HT)_2$ have a smaller number of particles, including some intercalated stacks, than those from the other two organoclays as shown in Fig. 1(b). On the other hand, nanocomposites from $M_3(HT)_1$ and $(HE)_2M_1T_1$ maintain a large number of particles with well-exfoliated structures even at high MMT concentrations as seen in Fig. 1(a) and (c). All the micrographs are supported by WAXS results that will be discussed later. The extent of organoclay exfoliation of these organoclays in a-PA is rather similar to that found for nylon 6. Apparently, a-PA, like nylon 6, has relatively good affinity for the polar surface of MMT; as expected, the two-tailed organic modifier ($M_2(HT)_2$) decreases the affinity of a-PA for the silicate surface by shielding the a-PA/MMT interactions and by creating a more hydrocarbon-like environment at the MMT surface than the one-tailed organic modifier. Due to the potential for interaction between the hydroxyl groups of the modifier ($(HE)_2M_1T_1$) with a-PA, the TEM micrographs of the two nanocomposites at both high and low MMT contents shown in Fig. 1(a) and (c) reveal well-exfoliated structures [8,11,15].

3.1.2. Particle analysis

The qualitative assessments from images like Fig. 1 described above can be quantified by particle analysis of these TEM micrographs; the statistical results are shown in Table 2. The experimentally determined MMT concentration of each nanocomposite after incineration is also shown in Table 2. According to Table 2, the average particle lengths for all these nanocomposites are slightly larger than those observed for nylon 6 nanocomposites, where almost all the particles are exfoliated, i.e., substantially ideal exfoliation [5,38]. For the nanocomposites based on a-PA, the average particle thicknesses and lengths of nanocomposites from $M_2(HT)_2$ are generally larger than those from $M_3(HT)_1$ and $(HE)_2M_1T_1$ while the average particle aspect ratios of nanocomposites from $M_3(HT)_1$ and $(HE)_2M_1T_1$ are generally larger than those from $M_2(HT)_2$ over the range of MMT concentrations. We also note that the aspect ratios obtained from the average values of each particle, $\langle l/t\rangle_n$ and $\langle l/t\rangle_w$, are generally larger than those calculated from the ratio of the corresponding average values of length and thickness, $(\bar{l}_n/\bar{t}_n)$ and $(\bar{l}_w/\bar{t}_w)$. The ratio of number average particle length and thickness, $(\bar{l}_n/\bar{t}_n)$, is always larger than the ratio of weight average particle length and thickness, $(\bar{l}_w/\bar{t}_w)$, while the weight average aspect ratio obtained by averaging values of each particle, $\langle l/t\rangle_w$, is always larger than the corresponding number average ratio, $\langle l/t\rangle_n$. This result is in a good agreement with our previous reports [13,21,31]. In addition, the fraction of single platelets was calculated with the results from the particle analysis. Particles with a thickness of nearly 1 nm were

Table 2
Results of particle analysis of nanocomposites

Organoclay	Wt% MMT	Total number of particles	Number average particle length ($\bar{l}_n$, nm)	Number average particle thickness ($\bar{t}_n$, nm)	Weight average particle length ($\bar{l}_w$, nm)	Weight average particle thickness ($\bar{t}_w$, nm)	Number average aspect ratio ($\bar{l}_n/\bar{t}_n$)	Number average aspect ratio $\langle l/t\rangle_n$	Weight average aspect ratio ($\bar{l}_w/\bar{t}_w$)	Weight average aspect ratio $\langle l/t\rangle_w$
$M_3(HT)_1$	1.57	323	115.4	2.6	142.5	3.8	44.7	54.7	37.1	74.0
	3.53	255	123.8	3.2	148.3	7.0	38.2	54.4	21.2	72.8
	5.56	739	96.7	2.4	117.9	4.9	41.1	53.7	24.2	71.4
	8.29	253	129.3	3.8	161.9	7.7	33.8	50.2	20.9	71.4
$M_2(HT)_2$	1.64	205	116.2	4.2	141.4	7.7	27.6	43.2	18.4	67.6
	3.16	281	133.3	5.8	165.2	13.0	22.9	41.7	12.7	68.2
	5.52	673	179.1	9.3	234.4	17.3	19.3	36.1	13.5	69.2
	8.14	267	145.8	6.3	194.4	11.5	23.0	37.7	16.9	67.7
$(HE)_2M_1T_1$	1.46	192	125.4	3.7	154.3	7.8	33.6	50.0	19.8	73.8
	3.19	250	118.4	3.2	145.7	6.5	37.4	50.7	22.4	67.4
	6.14	950	109.7	3.1	140.5	6.5	35.2	49.7	21.8	72.0
	8.85	265	102.9	2.9	126.5	6.0	35.8	47.5	21.1	63.0

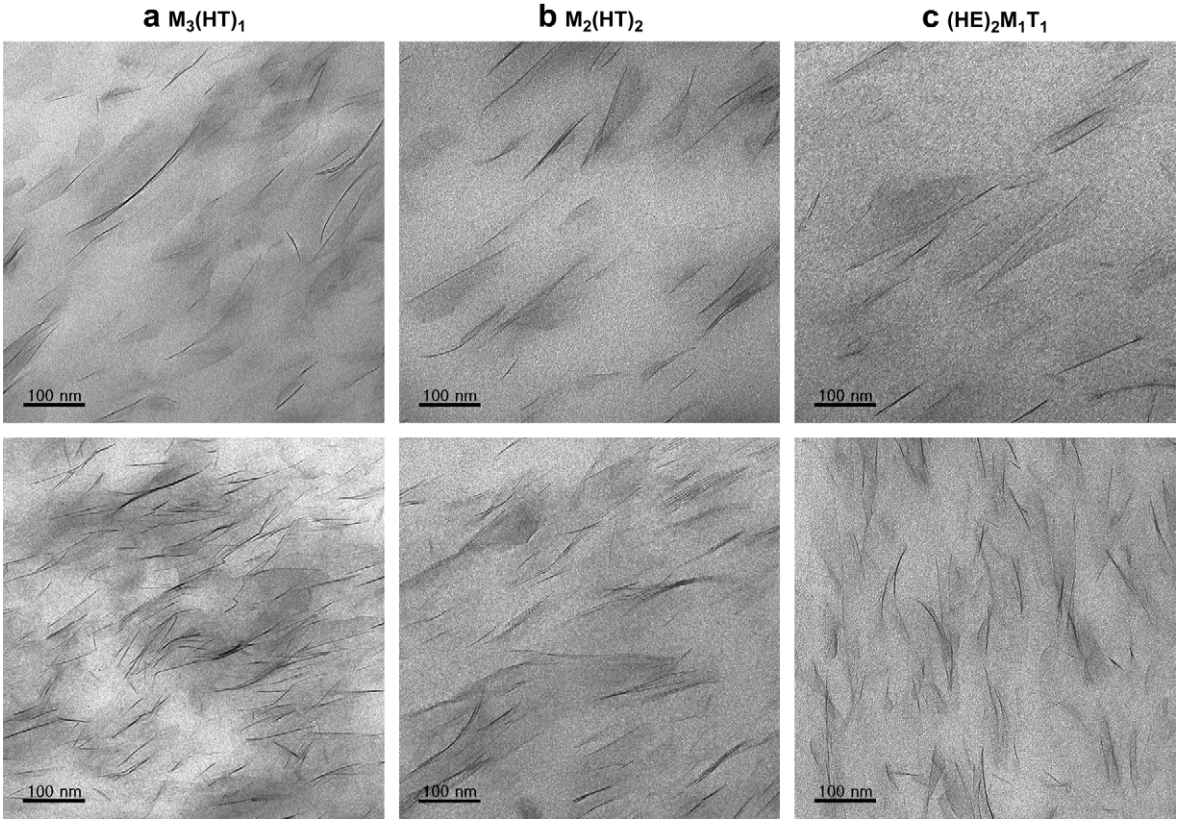

Fig. 1. TEM photomicrographs of nanocomposite based on a-PA and organoclays: (a) $M_3(HT)_1$, (b) $M_2(HT)_2$, and (c) $(HE)_2M_1T_1$; with concentrations ranging from ~1.5 wt% MMT (above) and ~5 wt% MMT (below).

considered as single platelets and the number of such particles was divided by the total number of particles to obtain the fraction shown in Fig. 2. Nanocomposites from $M_3(HT)_1$ and $(HE)_2M_1T_1$ have a higher fraction of single platelets than those from $M_2(HT)_2$ for all MMT concentrations. These trends are in a good agreement with the morphology analysis and mechanical properties that will be discussed later. Figs. 3 and 4 show a series of representative histograms of particle length, thickness, and aspect ratio obtained from TEM analysis for a-PA nanocomposites. Features for particle thickness and length show broader distributions based in

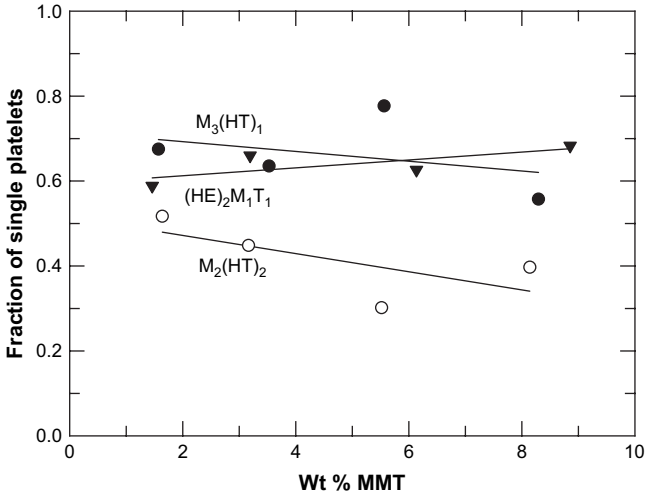

Fig. 2. Fraction of single platelet of organoclays for nanocomposites with various concentrations.

nanocomposites from $M_2(HT)_2$ than in those from $M_3(HT)_1$ and $(HE)_2M_1T_1$ as shown in Fig. 3. From Fig. 4, MMT particles with aspect ratios greater than 50 are more numerous in nanocomposites from $M_3(HT)_1$ and $(HE)_2M_1T_1$ than nanocomposites from $M_2(HT)_2$. The average thickness, length, and aspect ratio values from particle analyses from Figs. 3 and 4 and Table 2 are plotted in Figs. 5 and 6 versus MMT content of the nanocomposites. The average thickness and length of clay particles in nanocomposites from $M_2(HT)_2$ are significantly higher than in nanocomposites from $M_3(HT)_1$ and $(HE)_2M_1T_1$ while the opposite is true for the average aspect ratio of nanocomposites. The fact that the particle lengths are shorter in the more well-exfoliated composites than in the more poorly dispersed cases like those from $M_2(HT)_2$ organoclay can be explained by the fact that the platelets in tactoids are not stacked in registry as in a deck of cards but more disordered laterally.

3.1.3. *Wide angle X-ray scattering*

WAXS is a commonly used technique for characterizing the exfoliation structure of nanocomposites. WAXS scans for the three corresponding pristine organoclays are included and shown at the bottom of Fig. 7 for comparison; the scans for the various nanocomposites have been shifted by successive increments to view them more clearly. Moreover, to compare the structure between the skin and the core, some specimens were precision milled to half depth of the original bar thickness. Comparing the scans for the skin, nanocomposites from $M_3(HT)_1$ and $(HE)_2M_1T_1$ have no characteristic X-ray diffraction peaks as may be seen in Fig. 7(a) and (c), which suggests a highly exfoliated structure. Nanocomposites from $M_2(HT)_2$, on the other hand, have a peak at approximately $2\theta = 2.56^\circ$, which corresponds to an interlayer spacing of 34.5 Å. This spacing is approximately 10.3 Å larger than the basal spacing of the neat $M_2(HT)_2$ organoclay, indicating the presence of

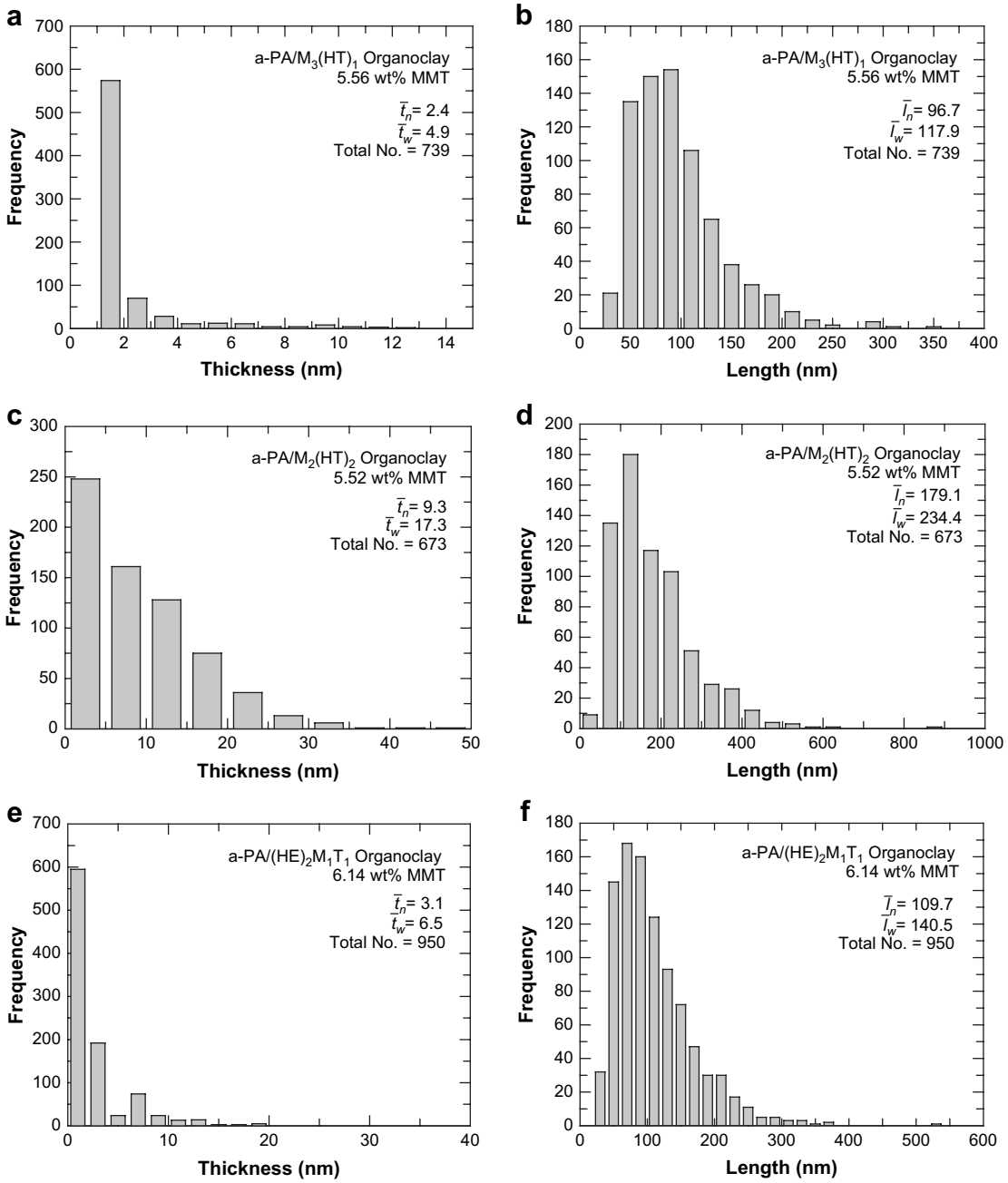

Fig. 3. Histograms of thicknesses (left) and lengths (right) for a-PA/organoclay nanocomposites: (a,b) $M_3(HT)_1$ (c,d) $M_2(HT)_2$ and (e,f) $(HE)_2M_1T_1$.

a population of intercalated structures. These results are in a good agreement with TEM micrographs and our previous report on nylon 6 nanocomposites [8,11]. WAXS scans from the core of these nanocomposites are quite different from the skin in that no characteristic X-ray diffraction peaks are observed for the samples made from any of the organoclays. This result implies that there are distinct structural differences between the skin and core of injection-molded specimens of nanocomposites based on a-PA and three different kinds of organoclays. It is not reasonable to attribute these observations to differences in exfoliation levels from the skin to the core; it is more likely that the clay particles are more oriented in the skin than the core as suggested by Lee et al. [14]. Apparently, the lack of a diffraction peak from the tactoids in the core at this sensitivity reflects their disorder. Actually, the WAXS results provide only limited information about morphology while direct observation by TEM provides a more clear understanding of exfoliation levels. Of course, for TEM the observed area is rather small and a given image might not be representative of the nanocomposite as a whole. Thus, it is necessary to analyze multiple images to gain a full understanding of the morphology. Measurement of bulk properties such as mechanical, thermal and dynamic mechanical properties complements TEM and WAXS analyses [13,31].

3.2. Mechanical properties

The type and amount of organoclay added to a-PA significantly affects the mechanical properties observed. Fig. 8 shows representative stress–strain curves for a-PA and its nanocomposites prepared from $M_2(HT)_2$. The yield points for these materials,

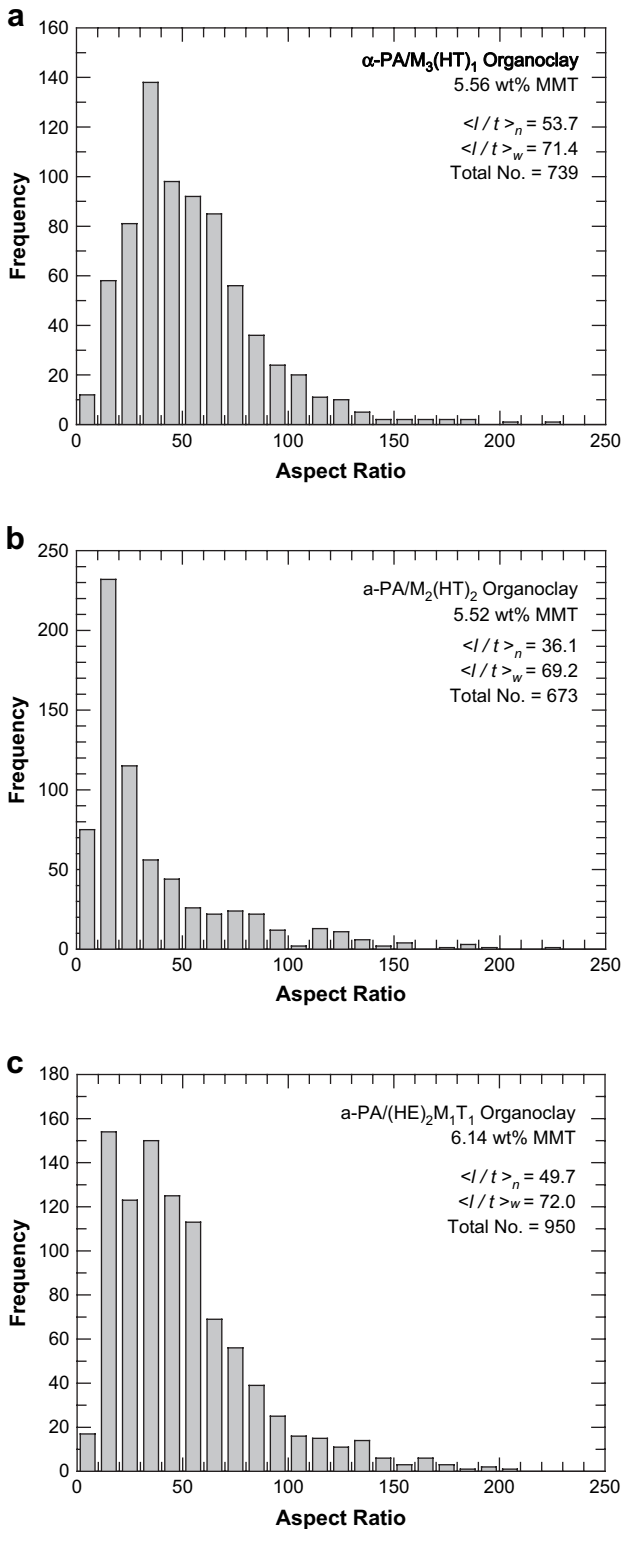

Fig. 4. Histograms of aspect ratios for a-PA/organoclay nanocomposites: (a) $M_3(HT)_1$ (b) $M_2(HT)_2$ and (c) $(HE)_2M_1T_1$.

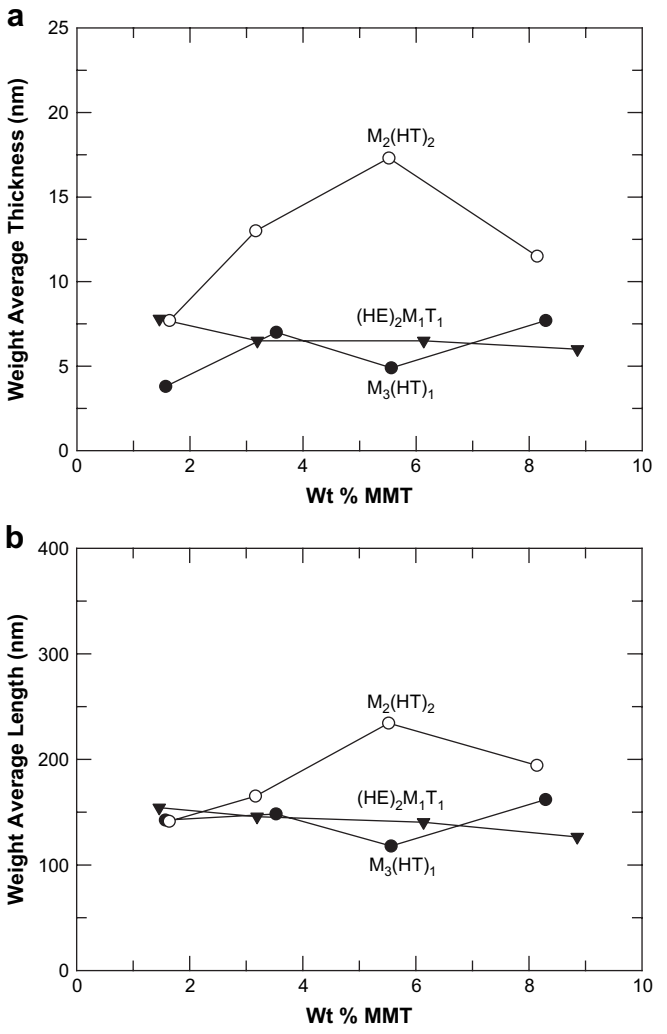

Fig. 5. Weight average thicknesses (a) and lengths (b) of nanocomposite based on a-PA.

defined as the highest stress at which $d\sigma/d\varepsilon = 0$, increase with MMT concentration. The deformation behavior after the yield point is strongly affected by MMT concentration and elongation at break decreases with MMT concentration.

Fig. 9(a) shows the effect of MMT concentration on the tensile modulus of nanocomposites prepared from a-PA and the organoclays, $M_3(HT)_1$, $M_2(HT)_2$ and $(HE)_2M_1T_1$. Nanocomposites from the one-tailed organoclay, $M_3(HT)_1$, which have a well-exfoliated structure, exhibit the highest level of stiffness enhancement; whereas, those based on the two-tailed organic modifier, $M_2(HT)_2$, exhibit the lowest degree of reinforcement. This agrees with the morphological results mentioned above and is similar to what was observed for nylon 6 nanocomposites [8,11]. Of the various mechanical properties, modulus provides the best indicator of organoclay exfoliation and is, therefore, useful for quantitatively gauging effects of modifier structure on exfoliation [8]. Similar trends are observed for the yield strength as shown in Fig. 9(b). The elongation at break data, presented in Fig. 9(c), decreases, as expected, with the addition of MMT; the more exfoliated nanocomposites from $M_3(HT)_1$ and $(HE)_2M_1T_1$ are less ductile than the nanocomposite from $M_2(HT)_2$. As shown in Fig. 10, the Izod impact strength for nanocomposites from $M_3(HT)_1$ and $(HE)_2M_1T_1$ remain at the level of neat a-PA. Nanocomposites from $M_2(HT)_2$, however, show somewhat higher Izod impact strength values than neat a-PA so long as the MMT content is less than 8 wt%. It should be noted that all the specimens failed in a brittle manner in this impact test. Like nylon 6, a-PA is a semi-ductile material in that it fails in a ductile manner in slow tensile tests but is brittle when notched and tested at high strain rates. The fracture energy recorded in an impact test reflects the integration of the resisting force of the sample over the range of the sample deflection. Adding clay increases the forces due to the high modulus and yield strength but

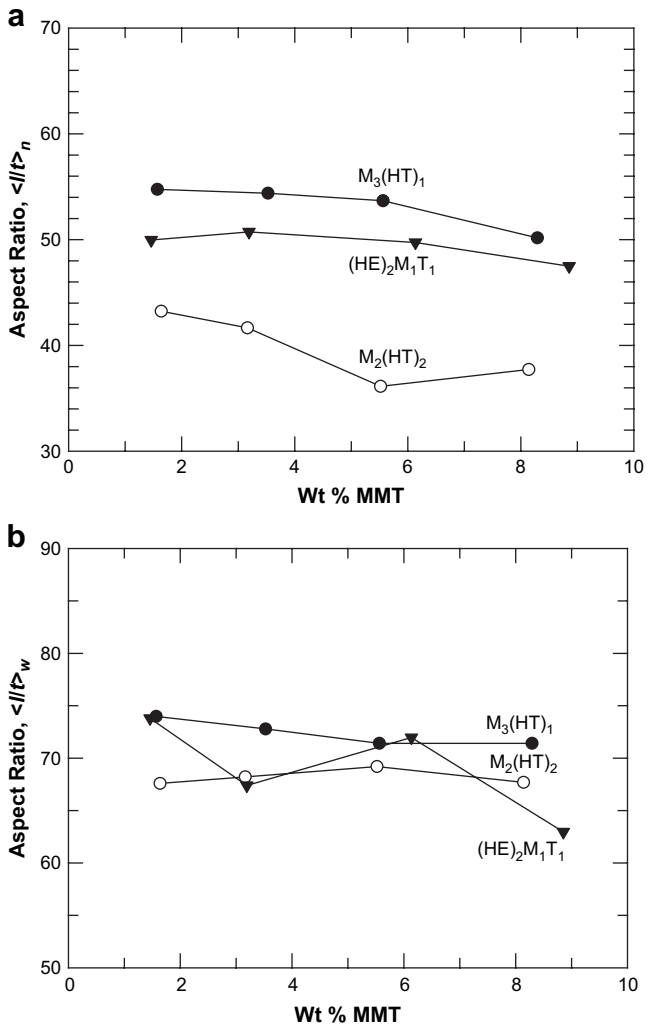

Fig. 6. Aspect ratios of nanocomposite based on a-PA: (a) $\langle l/t \rangle_n$ and (b) $\langle l/t \rangle_w$.

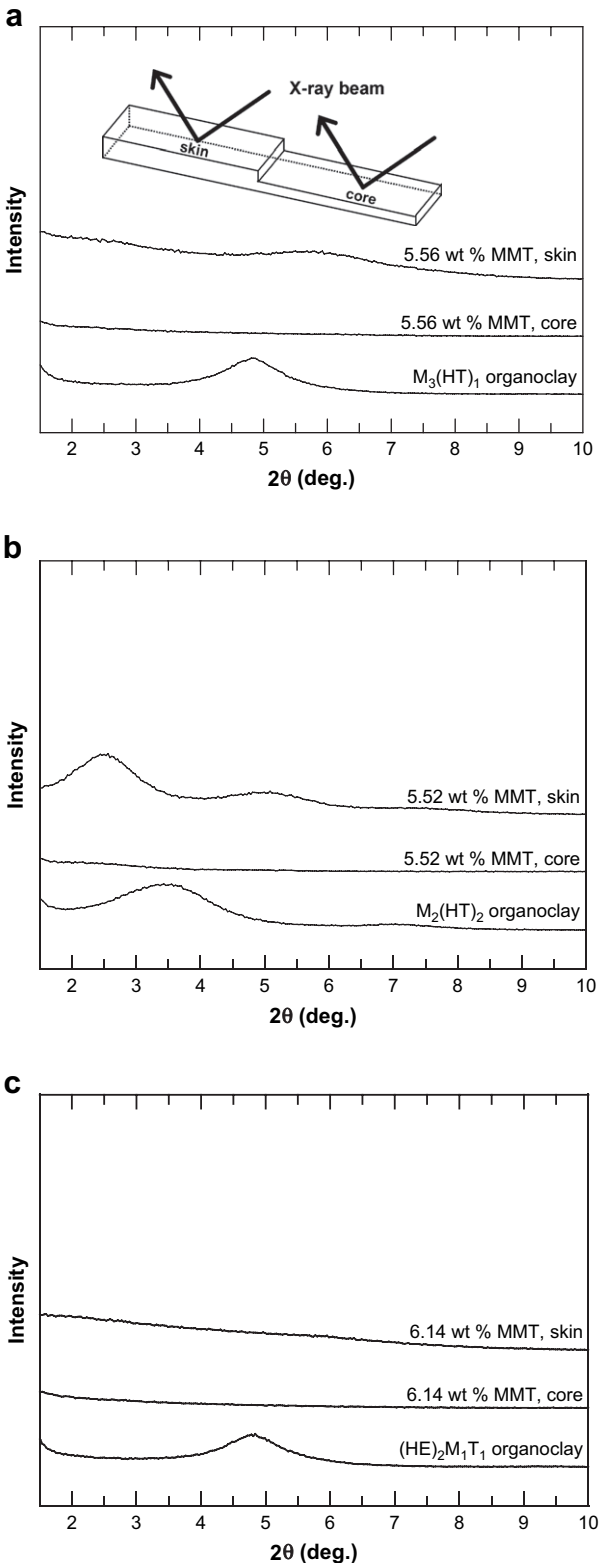

Fig. 7. Skin and core effects on WAXS patterns of pristine organoclays and nanocomposites: (a) $M_3(HT)_1$, (b) $M_2(HT)_2$, and (c) $(HE)_2M_1T_1$.

decreases the ductility. The extent of these changes varies with the type of organoclay as seen in Figs. 9 and 10. Generally, high levels of exfoliation tend to decrease the impact energy [6,7,9,34,35], however, in some cases the opposite can be observed owing to the balance of force versus deflection levels involved [15,39–41]. The increases for the $M_2(HT)_2$ nanocomposites may involve similar considerations.

3.3. Dynamic mechanical properties and prediction of heat distortion temperature

Fig. 11 shows the effect of MMT content and temperature on the dynamic mechanical properties of nanocomposites prepared from a-PA and $M_3(HT)_1$. As might be expected from the tensile test results discussed above, the storage modulus, E', increases with MMT content at all temperatures as shown in Fig. 11(a). The largest increase in storage modulus is seen near the glass transition region, T_g, of a-PA because the relative reinforcement effect becomes greater as the a-PA modulus decreases in going from the glassy state to the rubbery state [38,42]. MMT, however, remains rigid over this temperature change. So, the reinforcing effect of MMT in a-PA matrix is enhanced above T_g. Fig. 11(b) shows the effects of MMT content and temperature on tan δ. The tan δ curves are shifted slightly to higher temperatures as MMT is added. However, this does not reasonably mean that T_g has shifted to higher temperatures. Furthermore, it is noteworthy that the height of the tan δ decreases and the curve broadens with MMT content in the vicinity of T_g. Since the three parameters E', E'', and tan δ are related by $\tan \delta = E''/E'$, the low tan δ values for the nanocomposites are mainly a result of larger changes of the E' in the T_g region than those

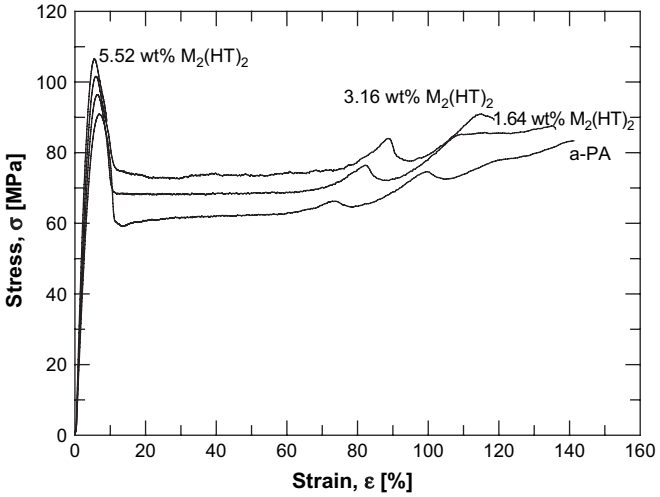

Fig. 8. Stress–strain behavior of a-PA and its nanocomposites containing $M_2(HT)_2$ with various concentrations.

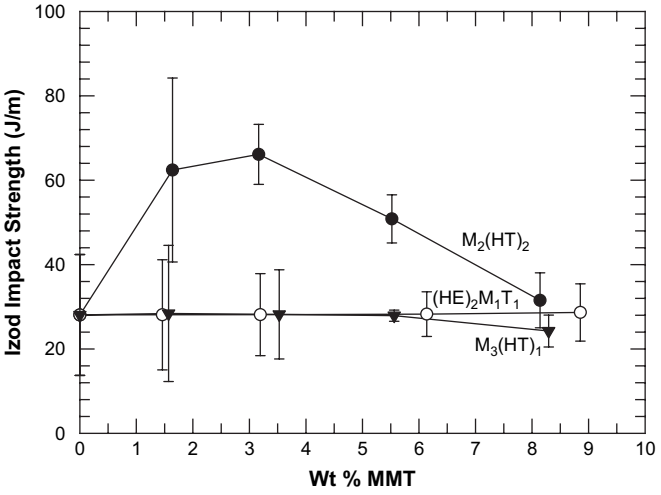

Fig. 10. Izod impact strength of nanocomposite based on a-PA containing $M_3(HT)_1$, $M_2(HT)_2$, and $(HE)_2M_1T_1$ organoclays.

of the E'' (Fig. 11(c)) [38,43,44]. Actually, the difference between the E'' peaks is much smaller than that between the tan δ peaks in the vicinity of T_g. The E'' peak shifts to slightly higher temperatures with addition of organoclay as shown in Table 3.

As mentioned above, the heat distortion temperature, HDT, of a polymer, as defined by ASTM D648, can be approximated from DMTA results like those in Fig. 12 [37]. In the ASTM method for HDT measurement, a bar specimen with a rectangular crosssection is

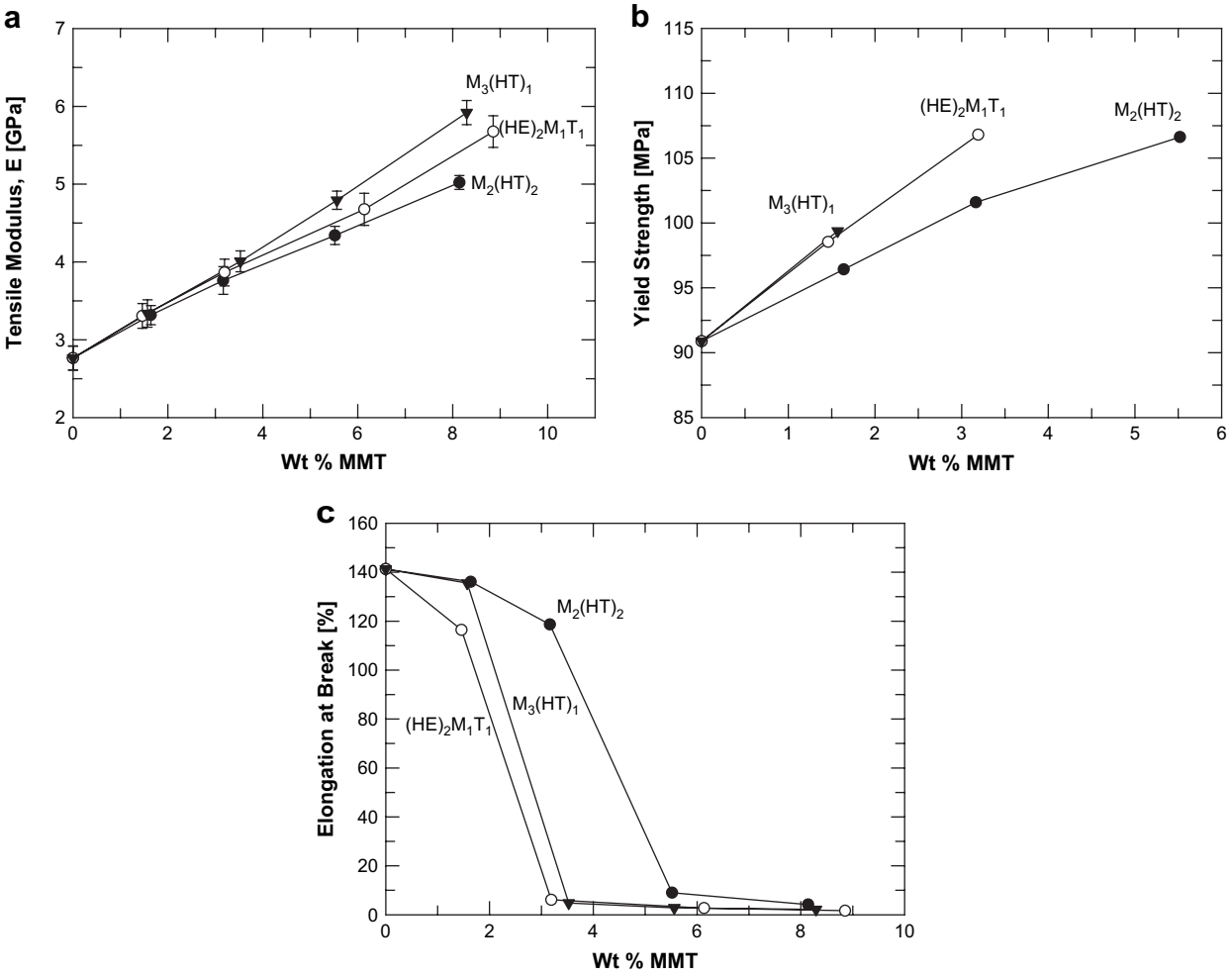

Fig. 9. Mechanical properties of nanocomposites based on a-PA containing $M_3(HT)_1$, $M_2(HT)_2$, and $(HE)_2M_1T_1$ organoclays: (a) tensile modulus, (b) yield strength and (c) elongation at break.

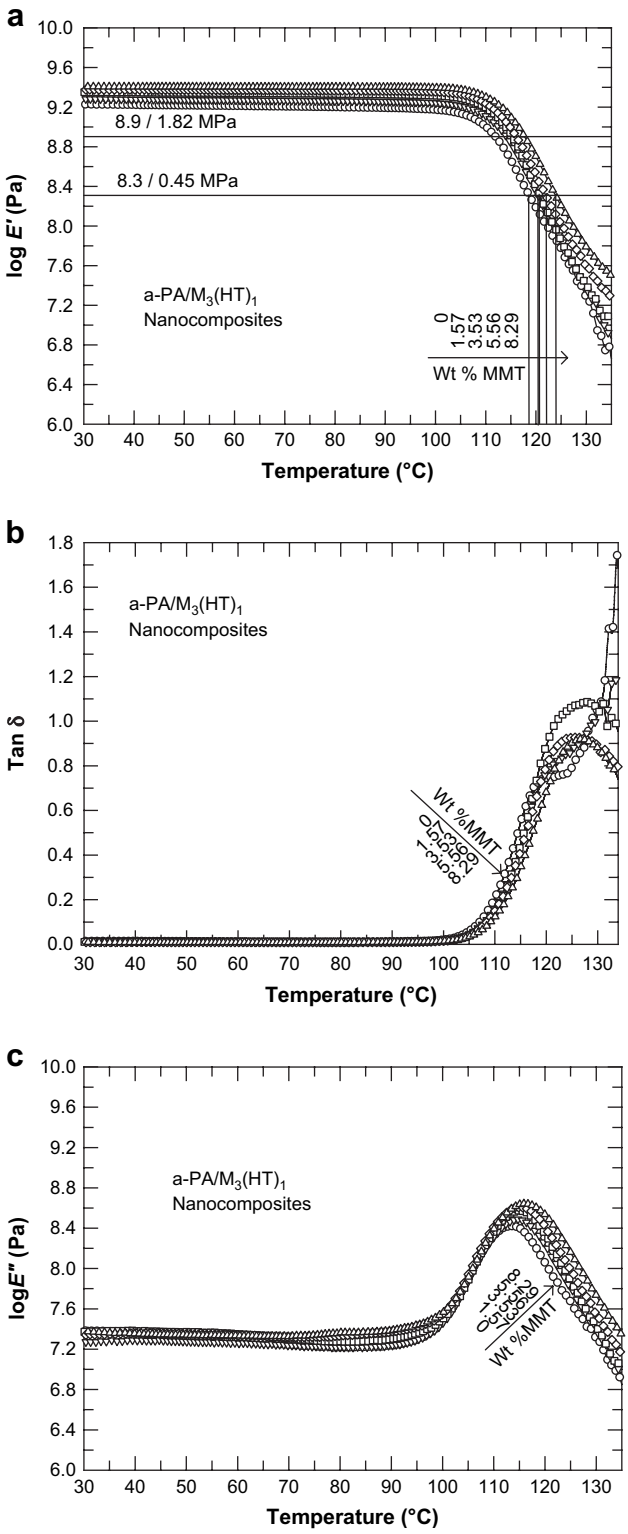

Fig. 11. Dynamic mechanical data for a-PA/$M_3(HT)_1$ nanocomposite containing $M_3(HT)_1$: (a) storage modulus, E', (b) tan δ, and (c) loss modulus, E''. The technique used for estimating the heat distortion temperature is illustrated in the plot of log E' versus temperature.

tested as a beam simply supported at both ends, with the load placed at its center. The load provides a maximum fiber stress of 0.45 or 1.82 MPa. Temperature is increased at 2 °C/min, and the point at which the bar specimen deflects 0.25 mm is recorded as the HDT (ASTM D648). If one draws a horizontal line at approximately 8.3 or 8.9 on the log E' axis, the intersection with the E' curve will correspond to the HDT, read directly from the x-axis [37,38]. Fig. 12 and Table 3 show the HDT values deduced in this way at the two stress levels specified by ASTM for nanocomposites made from $M_3(HT)_1$. At 0.45 MPa, the HDT for the neat a-PA is about 119 °C which is similar to the value obtained by the ASTM HDT test. The addition of 8 wt% MMT increases the HDT to about 124 °C, however, for nylon 6 nanocomposites, the HDT was increased from 55 to 160 °C with addition of 8 wt% MMT. The large increase in HDT for nylon 6 is the result of the shape of the modulus versus temperature curve and the increase in modulus by addition of the filler. Since nylon 6 is semi-crystalline polymer, some level of stiffness can be maintained beyond T_g and up to T_m [38]. However, a-PA is amorphous and goes directly from the glassy state to the rubbery state above T_g; this is evident by the shape of the log E' versus temperature curve in Fig. 12. It has been repeatedly shown that fillers typically increase the HDT of semi-crystalline polymers much more effectively than for amorphous polymers [44].

Table 3
T_g and HDT results for $M_3(HT)_1$ organoclay nanocomposites based on amorphous PA

Wt% MMT	T_g[a] (°C)	HDT (°C) at low load	HDT (°C) at high load
0	113.6	118.7	112.0
1.57	114.7	120.6	114.2
3.53	114.8	120.9	115.3
5.56	115.1	122.1	116.1
8.29	115.9	124.0	117.8

[a] Glass transition temperature, T_g, was determined from the major peak of the loss modulus, E'' [43].

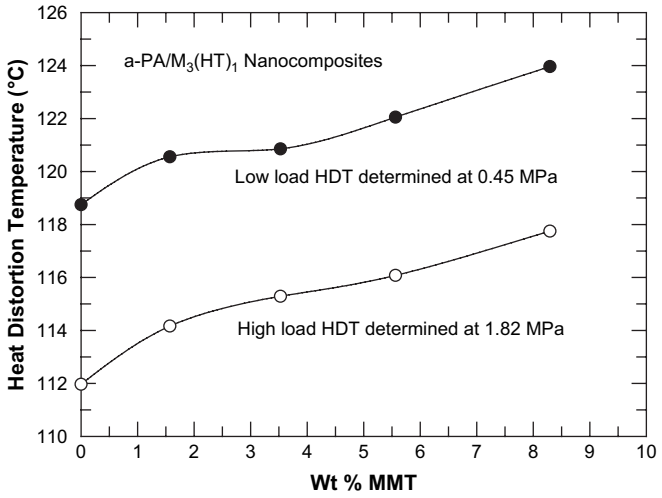

Fig. 12. Effect of MMT concentration on the heat distortion temperature of nanocomposites containing $M_3(HT)_1$. Data were collected from the plot of log E' versus temperature.

4. Conclusion

Nanocomposites based on a commercial amorphous polyamide designated here as a-PA and three organoclays, $M_3(HT)_1$, $M_2(HT)_2$ and $(HE)_2M_1T_1$, were prepared by melt processing to explore the effect of the organoclay structure on the morphology and properties of these nanocomposites. The structure of these nanocomposites was evaluated by WAXS and TEM, including a detailed particle analysis for quantitative assessment. Tensile properties, impact fracture behavior and dynamic mechanical properties were determined. Morphology analyses show that a one-tailed organoclay, $M_3(HT)_1$, and an organoclay containing hydroxyl ethyl groups, $(HE)_2M_1T_1$, give well-exfoliated structures while nanocomposites

from the two-tailed organoclay, $M_2(HT)_2$, contain a high concentration of intercalated stacks. Nanocomposites from $M_3(HT)_1$ lead to slightly better exfoliation than those from $(HE)_2M_1T_1$. The fraction of single platelets is larger in nanocomposites from $M_3(HT)_1$ and $(HE)_2M_1T_1$ than in nanocomposites from $M_2(HT)_2$. Mechanical property tests show that $M_3(HT)_1$ produces the highest matrix reinforcement as reflected by the tensile modulus and yield strength. It appears that a-PA, like nylon 6, has good affinity for the pristine silicate surface of the clay leading to better exfoliation with $M_3(HT)_1$ than with multiple-tailed organic modifiers. Multiple-tailed organic modifiers shield the MMT surface more than the one-tailed organic modifier which hinders the desirable polar a-PA/polar MMT surface interaction. As a result, surfactants with multiple tails lead to a less exfoliated structure. Of the three organoclays, the one-tailed organoclay, $M_3(HT)_1$, seems to provide an optimum combination of these effects, since the best exfoliation and the highest mechanical properties are achieved for a-PA.

Acknowledgements

The authors sincerely thank P. J. Yoon and D. L. Hunter of Southern Clay Products, Inc. for providing organoclay materials, and many helpful discussions.

References

[1] Vaia RA, Maguire JF. Chem Mater 2007;19(11):2736–51.
[2] Krishnamoorti R, Vaia RA. J Polym Sci Part B Polym Phys 2007;45(24):3252–6.
[3] Chavarria F, Paul DR. Polymer 2006;47(22):7760–73.
[4] Yoo Y, Kim S-S, Won JC, Choi K-Y, Lee JH. Polym Bull 2004;52(5):373–80.
[5] Chavarria F, Paul DR. Polymer 2004;45(25):8501–15.
[6] Cho JW, Paul DR. Polymer 2001;42(3):1083–94.
[7] Fornes TD, Paul DR. Macromolecules 2004;37(20):7698–709.
[8] Fornes TD, Yoon PJ, Hunter DL, Keskkula H, Paul DR. Polymer 2002;43(22):5915–33.
[9] Fornes TD, Yoon PJ, Keskkula H, Paul DR. Polymer 2001;42(25):9929–40.
[10] Noda N, Lee Y-H, Bur AJ, Prabhu VM, Snyder CR, Roth SC, et al. Polymer 2005;46(18):7201–17.
[11] Fornes TD, Hunter DL, Paul DR. Macromolecules 2004;37(5):1793–8.
[12] Hotta S, Paul DR. Polymer 2004;45(22):7639–54.
[13] Kim DH, Fasulo PD, Rodgers WR, Paul DR. Polymer 2007;48(18):5308–23.
[14] Lee H-S, Fasulo PD, Rodgers WR, Paul DR. Polymer 2005;46(25):11673–89.
[15] Shah RK, Hunter DL, Paul DR. Polymer 2005;46(8):2646–62.
[16] Granado A, Eguiazábal JI, Nazábal J. Macromol Mater Eng 2004;289(3):281–7.
[17] Koriyama H, Oyama HT, Ougizawa T, Inoue T, Weber M, Koch E. Polymer 1999;40(23):6381–93.
[18] Liu Y, Donovan JA. Polymer 1995;36(25):4797–803.
[19] Garcia A, Eceolaza S, Iriarte M, Uriarte C, Etxeberria A. J Membr Sci 2007;301(1-2):190–9.
[20] Zheng W, Lee YH, Park CB. J Cell Plast 2006;42(4):271–88.
[21] Cui L, Ma X, Paul DR. Polymer 2007;48(21):6325–39.
[22] Han SS, Kim YS, Lee S-G, Lee JH, Zhang K, Choi HJ. Macromol Symp 2006;245–246(1):199–207.
[23] Kim DH, Cho KS, Mitsumata T, Ahn KH, Lee SJ. Polymer 2006;47(16):5938–45.
[24] Min KD, Kim MY, Choi K-Y, Lee JH, Lee S-G. Polym Bull 2006;57(1):101–8.
[25] Sung YT, Kim YS, Lee YK, Kim WN, Lee HS, Sung JY, et al. Polym Eng Sci 2007;47(10):1671–7.
[26] Yoo Y, Park C, Lee S-G, Choi K-Y, Kim DS, Lee JH. Macromol Chem Phys 2005;206(8):878–84.
[27] Huang JJ, Keskkula H, Paul DR. Polymer 2004;45(12):4203–15.
[28] Huang JJ, Keskkula H, Paul DR. Polymer 2006;47(2):624–38.
[29] Ahn Y-C, Paul DR. Polymer 2006;47(8):2830–8.
[30] Kelnar I, Kotek J, Kaprálková L, Munteanu BS. J Appl Polym Sci 2005;96(2):288–93.
[31] Kim DH, Fasulo PD, Rodgers WR, Paul DR. Polymer 2007;48(20):5960–78.
[32] Tjong SC, Bao SP. J Polym Sci Part B Polym Phys 2005;43(5):585.
[33] Xanthos M, Parmer JF, Forest MLL, Smith GR. J Appl Polym Sci 1996;62(8):1167–77.
[34] Yoon PJ, Hunter DL, Paul DR. Polymer 2003;44(18):5323–39.
[35] Stretz HA, Paul DR, Cassidy PE. Polymer 2005;46(11):3818–30.
[36] Yoon PJ, Fornes TD, Paul DR. Polymer 2002;43(25):6727–41.
[37] Paul DR, Bucknall CB. Polymer blends. New York: Wiley; 2000.
[38] Fornes TD, Paul DR. Polymer 2003;44(17):4993–5013.
[39] Chen L, Wong S-C, Liu T, Lu X, He C. J Polym Sci Part B Polym Phys 2004;42(14):2759–68.
[40] Wang K, Chen L, Wu J, Toh ML, He C, Yee AF. Macromolecules 2005;38(3):788–800.
[41] Yoo Y, Shah RK, Paul DR. Polymer 2007;48(16):4867–73.
[42] Huang JJ, Keskkula H, Paul DR. Polymer 2006;47(2):639–51.
[43] Locke CE, Paul DR. Polym Eng Sci 1973;13(4):308–18.
[44] Nielsen LE, Landel RF. Mechanical properties of polymers and composites. New York: Marcel Dekker; 1994.
[45] Ellis TS. Macromolecules 1991;24(13):3845–52.